Science
AAAS

Detection of Silica-Rich Deposits on Mars

S. W. Squyres *et al.*

Science **320**, 1063 (2008);
DOI: 10.1126/science.1155429

Science (print ISSN 0036-8075; online ISSN 1095-9203) is published weekly, except the last week in December, by the American Association for the Advancement of Science, 1200 New York Avenue NW, Washington, DC 20005.

measured at 247 points on 90 individual trees from 16 synthetic batches (Fig. 4C). To extract the magnitude of the Burgers vector, a line can be fit to the data as plotted, with the slope representing b from Eq. 1 above. This can be more directly seen in a histogram of the calculated Burgers vectors (Fig. 4D). A Gaussian fit to these data yields the average magnitude of the screw component of the Burgers vector $b = 6 \pm 2$ Å. Because the Burgers vector direction is confirmed to be [110] by TEM, a 6 Å screw component of the Burgers vector (the projection of **b** onto the dislocation line **u** [100]) is approximately equal to the lattice constant of PbS, $a = 5.94$ Å. It is known that smallest **b** allowable is the shortest lattice translation vector in a material (*23*), which in the case of rock salt crystals is $\frac{1}{2}\langle 110\rangle$, whose screw component is $\frac{1}{2}\langle 100\rangle$ (half the lattice constant a). Given various sources of errors in this estimate (*27*), it is satisfying to see that no data were observed substantially below the theoretical minimal vector, and the average estimated b value of twice the minimal theoretical length is reasonable. Additionally, theory predicts that left-handed dislocation spirals lead to right-handed Eshelby twists and vice versa (*23*, *26*); therefore, the equal probability of twist handedness implies equal probability of Burgers vector sense (sign).

The observation of Eshelby twist in these pine tree nanowires is a clear demonstration and validation of Eshelby's theory on dislocations. The results also provide evidence for a catalyst-free nanowire growth mechanism driven by axial screw dislocations and imply that VLS and screw dislocation-driven nanowire growth can coexist. Because of the distinct morphology difference from the hyperbranched nanowires, it is unlikely that the dislocation is a result of cool-down or other postgrowth perturbation. Although some general discussions on the origins of dislocations exist (*23*, *30*), an experimentally observed mechanistic understanding is currently lacking. We suggest that this dislocation-driven nanowire growth mechanism proposed for PbS trees is likely general to and is underappreciated in the synthesis of 1D nanostructures, particularly in cases where the growth mechanism is inconclusively explained and especially when free of catalysts. Besides the analogous PbSe for which we have found preliminary evidence of similar growth phenomena, the dislocation-driven nanowire growth mechanism is likely to occur in materials that are prone to have screw dislocations, such as SiC, GaN, ZnO, and CdS, both in vapor-phase growth and in solution-phase synthesis. However, we caution that postgrowth mechanical perturbation could work the dislocation out of the nanowires, and one might not be able to observe dislocations in the final nanowire products if samples are not handled properly.

References and Notes

1. Y. Xia *et al.*, *Adv. Mater.* **15**, 353 (2003).
2. C. M. Lieber, Z. L. Wang, *MRS Bull.* **32**, 99 (2006).
3. A. M. Morales, C. M. Lieber, *Science* **279**, 208 (1998).
4. R. S. Wagner, W. C. Ellis, *Appl. Phys. Lett.* **4**, 89 (1964).
5. Z. W. Pan, Z. R. Dai, Z. L. Wang, *Science* **291**, 1947 (2001).
6. T. J. Trentler *et al.*, *Science* **270**, 1791 (1995).
7. A. I. Persson *et al.*, *Nat. Mater.* **3**, 677 (2004).
8. K. A. Dick *et al.*, *Nat. Mater.* **3**, 380 (2004).
9. D. Wang, F. Qian, C. Yang, Z. H. Zhong, C. M. Lieber, *Nano Lett.* **4**, 871 (2004).
10. A. Dong, R. Tang, W. E. Buhro, *J. Am. Chem. Soc.* **129**, 12254 (2007).
11. Materials and methods are available as supporting material on *Science* Online.
12. M. J. Bierman, Y. K. A. Lau, S. Jin, *Nano Lett.* **7**, 2907 (2007).
13. J. Zhu *et al.*, *Nano Lett.* **7**, 1095 (2007).
14. M. Fardy, A. L. Hochbaum, J. Goldberger, M. M. Zhang, P. Yang, *Adv. Mater.* **19**, 3047 (2007).
15. J. B. Hannon, S. Kodambaka, F. M. Ross, R. M. Tromp, *Nature* **440**, 69 (2006).
16. W. K. Burton, N. Cabrera, F. C. Frank, *Nature* **163**, 398 (1949).
17. W. K. Burton, N. Cabrera, F. C. Frank, *Philos. Trans. R. Soc. London A* **243**, 299 (1951).
18. G. W. Sears, *Acta Metall.* **1**, 457 (1953).
19. G. W. Sears, *Acta Metall.* **3**, 361 (1955).
20. R. S. Wagner, W. C. Ellis, K. A. Jackson, S. M. Arnold, *J. Appl. Phys.* **35**, 2993 (1964).
21. D. R. Veblen, J. E. Post, *Am. Mineral.* **68**, 790 (1983).
22. D. B. Williams, C. B. Carter, *Transmission Electron Microscopy: A Textbook for Materials Science* (Plenum, New York, 1996), chaps. 22 and 25.
23. J. P. Hirth, J. Lothe, *Theory of Dislocations* (McGraw-Hill, New York, 1968).
24. A. Foitzik, W. Skrotzki, P. Haasen, *Physica Status Solidi A* **121**, 81 (1990).
25. E. Bauser, H. Strunk, *J. Cryst. Growth* **51**, 362 (1981).
26. J. D. Eshelby, *J. Appl. Phys.* **24**, 176 (1953).
27. Edge dislocations do not produce such distortions. Mixed dislocations can be evaluated as separate screw and edge components. When the cross section of the nanowire is not circular (which is often the case), the cross-section area can be used together with a small correction factor for this calculation. When the dislocation line is not at the center of the cylinder, a small correction factor is applied.
28. R. D. Dragsdorf, W. W. Webb, *J. Appl. Phys.* **29**, 817 (1958).
29. G. W. Sears, *J. Chem. Phys.* **31**, 53 (1959).
30. F. R. N. Nabarro, *Theory of Crystal Dislocations* (Oxford Univ. Press, London, 1967).

31. S. J. thanks NSF (CAREER DMR-0548232), Research Corporation Cottrell Scholar Award, DuPont Young Professor Grant, and 3M Nontenured Faculty Award for support. M.J.B. was partially supported by an Air Products Fellowship. We thank R. Selinsky for assistance with the illustrations in Fig. 2.

Supporting Online Material

www.sciencemag.org/cgi/content/full/1157131/DC1
Materials and Methods
Figs. S1 to S9
References
Movie S1

29 February 2008; accepted 16 April 2008
Published online 1 May 2008;
10.1126/science.1157131
Include this information when citing this paper.

Detection of Silica-Rich Deposits on Mars

S. W. Squyres,[1]* R. E. Arvidson,[2] S. Ruff,[3] R. Gellert,[4] R. V. Morris,[5] D. W. Ming,[5] L. Crumpler,[6] J. D. Farmer,[3] D. J. Des Marais,[7] A. Yen,[8] S. M. McLennan,[9] W. Calvin,[10] J. F. Bell III,[1] B. C. Clark,[11] A. Wang,[2] T. J. McCoy,[12] M. E. Schmidt,[12] P. A. de Souza Jr.[13]

Mineral deposits on the martian surface can elucidate ancient environmental conditions on the planet. Opaline silica deposits (as much as 91 weight percent SiO_2) have been found in association with volcanic materials by the Mars rover Spirit. The deposits are present both as light-toned soils and as bedrock. We interpret these materials to have formed under hydrothermal conditions and therefore to be strong indicators of a former aqueous environment. This discovery is important for understanding the past habitability of Mars because hydrothermal environments on Earth support thriving microbial ecosystems.

Opaline silica deposits are an indicator of past aqueous activity. Some regions of Mars exhibit a thermal infrared spectral signature that has been interpreted to result from coatings of amorphous silica on rocks (*1*, *2*), although this interpretation is not unique (*3*). Results from the Mars rover Opportunity have suggested that opaline silica could be present in sulfate-rich sedimentary rocks at Meridiani Planum (*4*). The rover Spirit recently investigated the Eastern Valley between Home Plate and the Mitcheltree/Low Ridge complex (Fig. 1) in Gusev crater. Here we describe the discovery of silica-rich deposits in the Eastern Valley and farther east near sulfate-rich soil deposits.

Home Plate consists of laminated–to–cross-bedded tephra that shows evidence for a volcanic explosive origin, including a bomb sag produced when an ejected ~4-cm clast fell into deformable ash deposits (*5*). Mitcheltree Ridge and Low Ridge, located east of Home Plate, are partially eroded synclinal structures that expose tephra deposits (including lapillistones) capped by a deposit of vesicular basalt boulders. Soils in the Inner Basin ~250 m to the north (Samra) and ~50 m to the east (Tyrone) (Figs. 1 and 2) of Home Plate contain hydrated ferric sulfate deposits (*6*, *7*). The mobility of ferric iron under apparently oxidizing conditions, leading to ferric sulfates and oxides, is suggestive of low pH con-

ditions (*8*–*10*), and both deposits are interpreted to have originated under hydrothermal, acid-sulfate conditions (*6*). Although hydrated ferric sulfates dominate these deposits, Alpha Particle X-ray Spectrometer (APXS) (*11*) data also indicate that the nonsulfate component is enriched in SiO_2 relative to nearby rocks and soils (*6*), and Miniature Thermal Emission Spectrometer (Mini-TES) (*12*) spectra show an absorption feature at ~475 cm^{-1} that may be associated with amorphous silica.

The floor of the Eastern Valley exposes buff-colored, platy outcrops that we interpret on the basis of their composition, mineralogy, and fine-scale texture to be volcanic ash deposits altered under oxidizing acid-sulfate–dominated conditions. These outcrops are covered in places by light-toned clasts and are found in close association with outcrops that show a distinctive nodular appearance (Fig. 2).

Mini-TES thermal emission spectra acquired for an outcrop (Tyrone nodules in Fig. 1) near the Tyrone light-toned soil deposit and for light-toned nodular outcrops within the Eastern Valley (Fig. 2) exhibit the spectral signature associated with high silica contents (Fig. 3A). Although the outcrops are partially covered by windblown soil, the spectra contain a distinctive vibrational absorption feature at ~475 cm^{-1}, which is interpreted to result from the Si-O bending mode, and another at ~1110 cm^{-1}, which is interpreted to be the Si-O stretching mode of opaline silica (*13*). The spectra are distinct from those of quartz or cristobalite (*13*). Correcting for soil and dust contamination enhances the depths of these features (Fig. 3B).

The spectra include a prominent absorption near ~1260 cm^{-1}. This feature is atypical of laboratory spectra of opaline silica, which usually display only a shoulder in this location. Previous work has demonstrated that the depth of this feature is a function of the incidence angle, because the longitudinal optic mode dominates the transverse optic mode as the incidence angle increases (*14*). We confirmed this behavior with laboratory emission measurements for both synthetic amorphous silica and natural opaline silica samples (fig. S1). With increasing emission angle (where 0° is normal to the surface), the feature transitions from a shoulder to a prominent emissivity minimum. Because Mini-TES observations are obtained at emission angles ranging from 40° to nearly 90°, the spectra of opaline silica should display this distinctive feature.

During a drive on martian solar day (or "sol") 1148 (*15*), the rover's inoperative right front wheel (*16*) excavated light-toned soil deposits (fig. S2). Mini-TES spectra for these deposits (Fig. 3A) show the spectral features associated with opaline silica, including a weak emissivity maximum near 1625 cm^{-1} that results from the bending mode of bound water (*17*). In addition, a relatively broad and deep emissivity minimum centered at ~950 cm^{-1} is present and is interpreted as a transparency feature that arises in fine-grained particulate material where multiple scattering accentuates an otherwise weak absorption (*18*). Panoramic Camera (Pancam) (*19*) near-infrared reflectance spectra of the light-toned, high-Si soil deposits and nodules also reveal a distinct absorption feature that is consistent with the presence of H_2O in hydrated minerals (*20*).

We used the Microscopic Imager (MI) (*21*), APXS, and Mössbauer Spectrometer (MB) (*22*) to investigate several rocks and soils in the Eastern Valley. One rock outcrop [Elizabeth Mahon (*23*), which coincides approximately with the

[1]Department of Astronomy, Space Sciences Building, Cornell University, Ithaca, NY 14853, USA. [2]Department of Earth and Planetary Sciences, Washington University, St. Louis, MO 63130, USA. [3]School of Earth and Space Exploration, Arizona State University, Tempe, AZ 85287, USA. [4]Department of Physics, University of Guelph, Guelph, Ontario, N1G 2W1, Canada. [5]NASA Johnson Space Center, Houston, TX 77058, USA. [6]New Mexico Museum of Natural History and Science, Albuquerque, NM 87104, USA. [7]NASA Ames Research Center, Moffett Field, CA 94035, USA. [8]Jet Propulsion Laboratory, California Institute of Technology, Pasadena, CA 91109, USA. [9]Department of Geosciences, State University of New York, Stony Brook, NY 11794, USA. [10]Department of Geological Sciences, University of Nevada, Reno, NV 89557, USA. [11]Lockheed Martin Corporation, Littleton, CO 80127, USA. [12]Department of Mineral Sciences, National Museum of Natural History, Smithsonian Institution, Washington, DC 20560, USA. [13]Tasmanian Information and Communication Technology Centre, Commonwealth Scientific and Industrial Research Organisation, Castray Esplanade, Hobart, TAS 7000, Australia.

*To whom correspondence should be addressed. E-mail: squyres@astro.cornell.edu

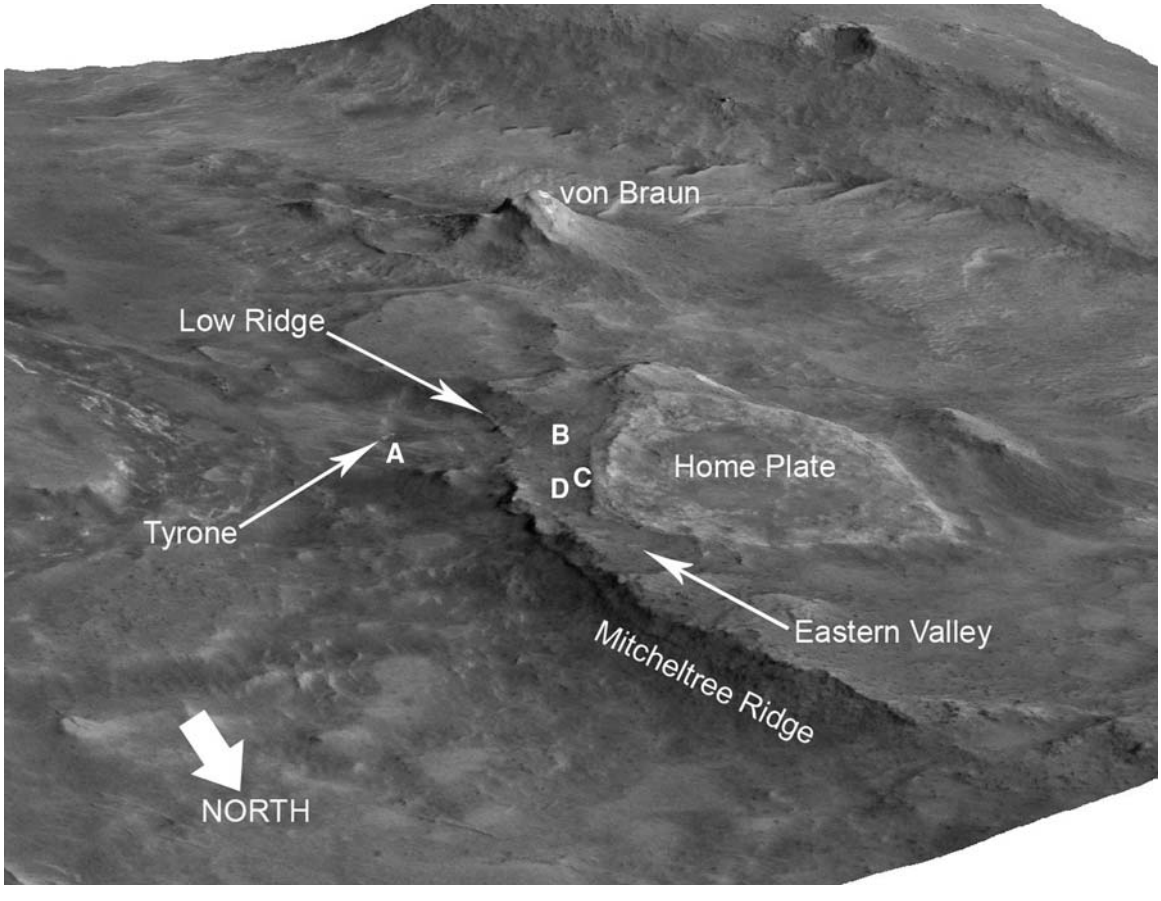

Fig. 1. Perspective view of the Inner Basin of the Columbia Hills. The Eastern Valley is the location of the silica-rich deposits, with the exception of an outcrop near Tyrone [(**A**), Tyrone nodules outcrop]. (**B**) Location of the Kobal outcrop (Fig. 2A), (**C**) location of the Elizabeth Mahon outcrop, and (**D**) location of Nancy Warren, Innocent Bystander, and Gertrude Weise (Fig. 2B). The distance between the southern end of Home Plate and von Braun Hill is ~120 m. Image was generated using the Mars Reconnaissance Orbiter High Resolution Imaging Science Experiment (HiRISE) image PSP_001777_1655_red and a digital elevation model produced from HiRISE data.

Clara_Zaph4 Mini-TES target] had 72.4 weight percent (wt %) SiO_2 (table S1). Light-toned soils exposed by the rover's right front wheel (Kenosha Comets and Lefty Ganote) (Fig. 2B and fig. S2) had SiO_2 concentrations of 90.1 and 74.6 wt %, respectively. Two rock samples (Innocent Bystander and Norma Luker) (Fig. 2B and fig. S3) with, respectively, 63.1 and 69.2 wt % SiO_2 were rock fragments several centimeters in size that were created by breaking an outcrop with the rover's right front wheel. The high-silica measurements were made on the freshly broken surfaces, demonstrating that the silica is present within the rock to a depth of at least several centimeters. Microscopic Imager images of all outcrop targets show varying degrees of soil contamination, so these SiO_2 concentrations should be regarded as lower limits.

The APXS sampling depth is ~5 to 10 μm in rock for low–atomic number elements such as Si and 50 to 100 μm for higher–atomic number elements (*11*). This depth dependence can be used to investigate whether high-Si targets have a thin cover of soil. Compared with typical soils at the Spirit site, the light-toned soils are enriched in Si, Ti, Cr, and Zn (Fig. 4). Most other major elements, however, follow an exponential downward trend in relative abundance with rising element atomic number. This trend is a clear indicator that soil grains are mixed into the surface of the silica-rich material. On the basis of MB measurements and the Mg/Al ratio in APXS data, we estimate that soil contaminates ~30% of the Kenosha Comets target. (A small quantity of an alteration product could also be present.) Removing the contaminants leads to an inferred composition of ~98 wt % SiO_2, ~1.5 wt % TiO_2, ~0.4 wt % Cr_2O_3, ~200 parts per million (ppm) Ni, and ~330 ppm Zn.

APXS data also show that this soil target is rich in Si to a depth of at least 300 μm by comparing the ratios of the Compton and Rayleigh scatter peaks of the primary excitation radiation for x-ray fluorescence. The cross sections responsible for these two peaks have different atomic-number dependencies (including a large dependency on oxygen), and they originate from depths of as much as 300 μm. The scatter peaks ratio is nearly a factor of 2 different than it is for typical soils but is consistent with the scatter peak of a pure SiO_2 sample measured by the flight instrument during APXS instrument calibration (fig. S4).

Further evidence that the material is rich in SiO_2 to at least a few hundred micrometers is provided by nearly featureless Mössbauer spectra. The MB instrument samples to a few hundred micrometers (*22*) and only detects minerals that contain Fe. The material is therefore Fe-poor over at least this depth range.

The light-toned soils were mixed by the action of the rover wheels to a depth of a few centimeters, so the APXS and MB results imply that the soil is silica-rich to at least this depth. Additionally, because MI images show that they are dominated by grains much smaller than a few hundred micrometers in size, the APXS and MB data also demonstrate that these are not grains of typical martian soil coated with silica.

We interpret the silica-rich materials identified by Spirit to have formed under hydrothermal conditions, because they are found in close association with volcanic materials [e.g., Home Plate (*5*)] and, in some cases, are intimately mixed with ferric sulfates that are also probably of hydrothermal origin (*6*). Origin in a lacustrine evaporitic setting is unlikely given the complete lack of evidence for standing or flowing surface water at the Spirit site (*24*).

On Earth, a range of processes can produce high concentrations of opaline silica in hydrothermal settings. These processes result from the high solubility of silica in aqueous systems under warm and alkaline conditions (*25*) but much lower solubility at low pH. At one extreme, abundant hot neutral-to-alkaline groundwaters dissolve silica from subsurface rocks and then precipitate it when they reach the surface and cool and evaporate, forming sinter deposits. At the other extreme, very low pH waters are formed by condensation of water vapor and acid gases, typically in volcanic settings and at low water/rock ratios. These acid condensates interact with precursor rock like basalt, leaching away most minerals but leaving the most insoluble constituents—notably silica—behind (*26*). As an intermediate case, hydrothermal sinter deposits can also form at pH 2 to 4 and high water/rock ratios (*27*).

The enrichment of Ti (and Cr) in the silica-rich materials discovered by Spirit may provide a constraint on their origin. Like silica, titanium dioxide is relatively insoluble at low pH. A straightforward explanation for our observations therefore is that acid-sulfate low pH waters dissolved basaltic precursor materials, concentrating the highly insoluble silica (probably as opal-A) and titanium dioxide (probably as anatase). Based on the composition of relatively unaltered basalts at Gusev,

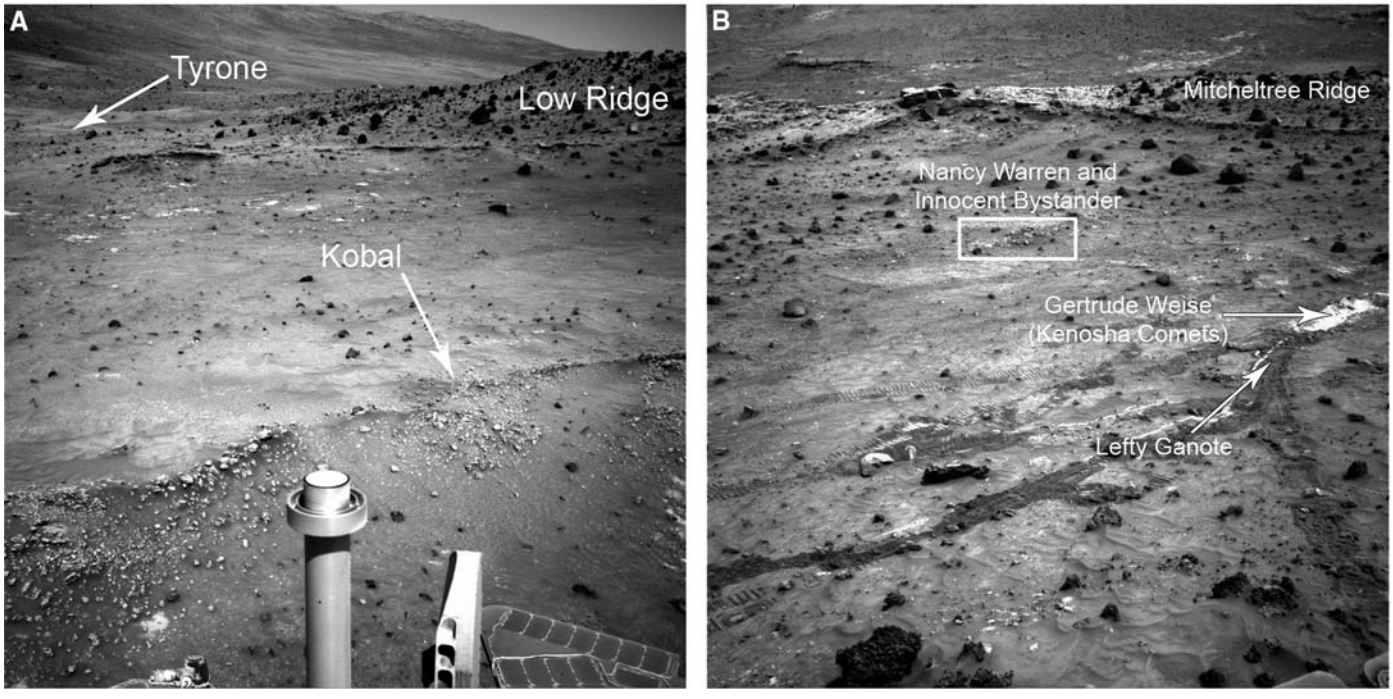

Fig. 2. (**A**) Navcam image acquired within the Eastern Valley, looking to the southeast and showing the nodular outcrop target Kobal that was examined with Mini-TES. The Tyrone area is shown before Spirit traversed there and exposed light-toned soils with its wheels. Navcam frame 2N195257205 acquired on sol 776. (**B**) Navcam image acquired in the Eastern Valley, looking west, showing the trench that was excavated by the front wheel and outcrops examined by the rover. Navcam frame 2N233253342 acquired on sol 1204.

titanomagnetite is the most likely precursor phase for the Ti.

Favoring a low pH origin is the similarity of silica-rich soils to other light-toned soil deposits within the Columbia Hills that are rich in hydrated sulfate salts, particularly ferric sulfates (*6*, *7*). Not only is their geologic setting similar—highly concentrated light-toned deposits excavated by the rover's wheels from just below the surface—but some of these sulfate-rich soils also contain a significant quantity (4 to 33%) of free silica (*6*). These observations may point toward a common origin, and as noted above, we interpret the hydrated ferric sulfate deposits to have formed under acid-sulfate conditions. Also, the compositional diversity of Si-rich materials observed by Spirit is consistent with formation by acid leaching of a variety of basaltic precursor materials, including those found in the Home Plate area (Fig. 5).

To remove nonvolatile components (e.g., Al, Fe, and Na) from the precursor rock, fluids—not vapors—are probably required. An unresolved issue is how far any fluids traveled before the most insoluble materials (SiO_2 and TiO_2) precipitated. If precipitation was local, at low water/rock ratios, the materials discovered by Spirit would most resemble the highly leached rocks and residual silica sometimes found in the vicinity of fumaroles (*26*, *28*). If there was considerable transport away from the source rocks before precipitation, implying higher water/rock ratios, the deposits would be more akin to the hydrothermal sinter deposits found at hot springs.

The composition of the Si-rich deposits does not uniquely constrain the pH of the fluids involved in their formation. For example, at high pH it is possible to precipitate sinter deposits from alkali chloride brines. Such precipitates are high in silica, and the presence of chloride can allow for elevated Ti levels as $TiCl_4$ or $TiOCl_2$ and the coprecipitation of anatase (*29*, *30*). Given the ample evidence for acid-sulfate processes elsewhere at Gusev, however, formation at low pH seems likely.

Hydrothermal conditions that produced high-purity opaline silica deposits on Mars could have led to locally habitable environments. Fumarolic environments and hot springs on Earth create habitable conditions for microbial life by conveying thermal waters, solutes, and volcanic gases to surface and near-surface environments (*31*, *32*) under both alkaline (*33*) and acidic (*31*, *34*) conditions. Any process that involves reprecipitation of silica from fluids can also provide a mechanism for preserving evidence of microbes (*35*). Whereas the silica-rich materials examined by Spirit are too small to be seen from orbit by current sensors, recent Compact Reconnaissance Imaging Spectrometer for Mars (*36*) observations of other regions on Mars may suggest the presence of more widespread and accessible hydrated and hydroxylated silica deposits elsewhere (*37*). Silica-rich deposits on Mars may be strong candidates for examination by future landed missions and as returned samples.

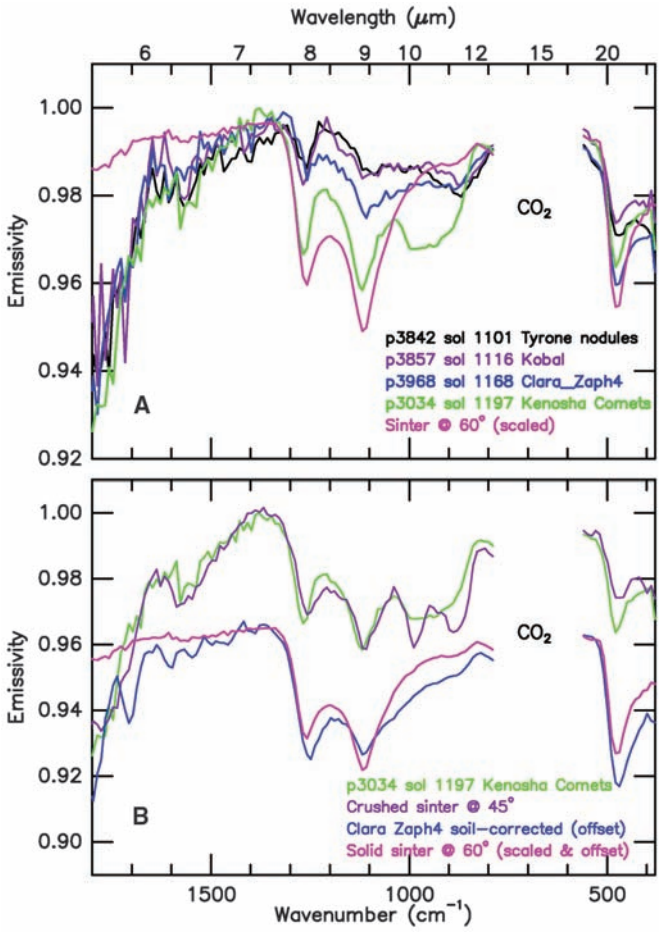

Fig. 3. (**A**) Mini-TES emissivity spectra for the outcrops Tyrone nodules, Kobal, Clara_Zaph4 (same location as the Elizabeth Mahon in situ target), and the soil Kenosha Comets. Also shown is a terrestrial opaline sinter acquired at an emission angle of 60° (similar to the Mini-TES observations). The notation pXXXX denotes the Mini-TES sequence identifier. (**B**) Comparison of a Mini-TES spectrum of Kenosha Comets with crushed hydrothermal sinter and comparison of a Mini-TES spectrum of the outcrop target Clara_Zaph4 (after correction for soil contamination) with solid hydrothermal sinter. All sinter samples are from Steamboat Springs, Nevada.

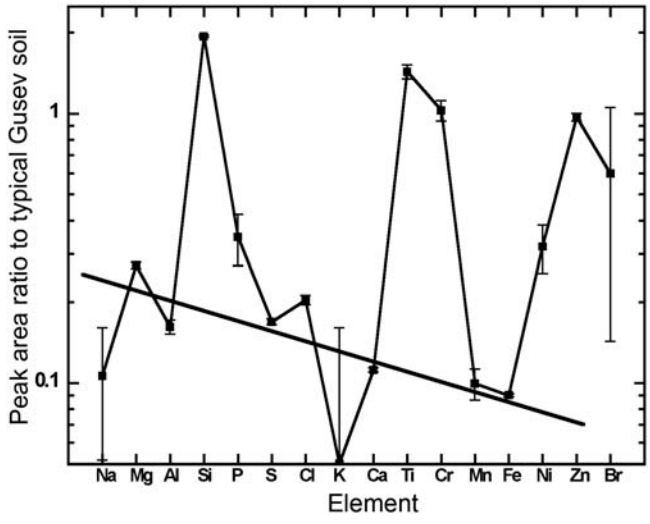

Fig. 4. Elemental composition of the bright soil deposit Kenosha Comets, ratioed on an element-by-element basis to typical Gusev soil. Si is strongly enriched relative to typical soil, and there are weaker enrichments in Ti, Cr, and Zn. Other major elements are strongly depleted relative to typical soil and exhibit an exponential decrease of relative abundance with increasing atomic number (diagonal line). Error bars indicate the 2σ statistical error in the Kenosha Comets sample.

References and Notes

1. M. D. Kraft *et al.*, *Geophys. Res. Lett.* **30**, 2288 (2003).
2. J. R. Michalski *et al.*, *Icarus* **174**, 161 (2005).
3. J. L. Bandfield, V. E. Hamilton, P. R. Christensen, *Science* **287**, 1626 (2000).
4. T. D. Glotch *et al.*, *J. Geophys. Res.* **111**, E12S06 (2006).
5. S. W. Squyres *et al.*, *Science* **316**, 738 (2007).
6. A. S. Yen *et al.*, *J. Geophys. Res.* **113**, E06S10 (2008).
7. J. R. Johnson *et al.*, *Geophys. Res. Lett.* **34**, L13202 (2007).
8. N. J. Tosca, A. Smirnov, S. M. McLennan, *Geochim. Cosmochim. Acta* **71**, 2680 (2007).
9. G. M. Marion, J. S. Kargel, D. C. Catling, *Geochim. Cosmochim. Acta* **72**, 242 (2008).
10. N. J. Tosca *et al.*, *J. Geophys. Res.*, 10.1029/2007JE003019.
11. R. Rieder *et al.*, *J. Geophys. Res.* **108**, 8066 (2003).
12. P. R. Christensen *et al.*, *J. Geophys. Res.* **108**, 8064 (2003).
13. J. R. Michalski *et al.*, *Geophys. Res. Lett.* **30**, 2008 (2003).
14. R. M. Almeida, *Phys. Rev. B* **45**, 161 (1992).
15. A martian solar day has a mean period of 24 hours, 39 min, and 35.244 s and is referred to as a "sol" to distinguish it from the shorter solar day on Earth. Spirit crossed from the Gusev plains to the Columbia Hills on the 157th sol after landing. Observations discussed in this paper were made over the period from sols 749 to 1288.
16. Spirit's right front wheel drive actuator failed on sol 799. Since then, the rover has mainly driven backward

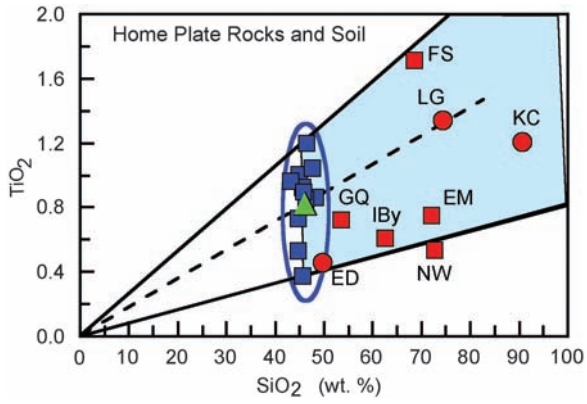

Fig. 5. Plot of titanium dioxide and silica contents for APXS measurements acquired since arriving at Home Plate and including observations from the Eastern Valley, Low Ridge, Mitcheltree Ridge, and the Tyrone areas. Red squares, silica-rich rocks; red circles, silica-rich soils; blue squares, basaltic rocks in the vicinity of Home Plate; and green triangle, typical local soil. The light blue region represents the compositions that can be obtained by acid-sulfate leaching of Home Plate rocks, assuming no variation in the TiO_2/SiO_2 ratio. KC, Kenosha Comets; LG, Lefty Ganote; FS, Fuzzy Smith; EM, Elizabeth Mahon; NW, Nancy Warren; ED, Eileen Dean; Iby, Innocent Bystander; and GQ, Good Question. The dashed line represents a typical evolutionary trend for leaching that preserves SiO_2 and TiO_2, and the blue oval indicates the range of basaltic rock compositions in the vicinity of Home Plate.

and dragged this nonrotating wheel along the surface, scraping paths through soils and crushing weak rocks.
17. J. W. Salisbury *et al.*, *Infrared (2.1-25 μm) Spectra of Minerals* (Johns Hopkins Univ. Press, Baltimore, 1991).
18. J. W. Salisbury *et al.*, *J. Geophys. Res.* **92**, 702 (1987).
19. J. F. Bell III *et al.*, *J. Geophys. Res.* **108**, 8063 (2003).
20. M. S. Rice *et al.*, Abstract #2138, presented at the 39th Annual Lunar and Planetary Science Conference, Houston, TX, 10 to 14 March 2008.
21. K. E. Herkenhoff *et al.*, *J. Geophys. Res.* **108**, 8065 (2003).
22. G. Klingelhöfer *et al.*, *J. Geophys. Res.* **108**, 8067 (2003).
23. Most of the rock and soil targets on the east side of Home Plate are named after players and teams from the All American Girls Professional Baseball League that operated from 1943 to 1954. The names are informal and not approved by the International Astronomical Union.
24. R. E. Arvidson *et al.*, *J. Geophys. Res.* **111**, E02S01 (2006).
25. P. M. Dove, J. D. Rimstidt, in *Silica: Physical Behavior, Geochemistry and Materials Applications*, P. J. Heaney, C. T. Prewitt, G. V. Gibbs, Eds. (Mineralogical Society of America, Washington, DC, vol. 29, 1994) pp. 259–308.
26. R. V. Morris *et al.*, *Lunar Planet. Sci.* **XXXI**, 2014 (2000).
27. K. A. Rodgers *et al.*, *Earth Sci. Rev.* **66**, 1 (2004).
28. K. A. Rodgers *et al.*, *Clay Miner.* **37**, 299 (2002).
29. H. D. Nam *et al.*, *Jpn. J. Appl. Phys.* **37**, 4603 (1998).
30. S. J. Kim, S. D. Park, Y. H. Jeong, *J. Am. Ceram. Soc.* **82**, 927 (1999).
31. W. P. Inskeep, T. R. McDermott, *Geothermal Biology and Geochemistry in Yellowstone National Park* (Thermal Biology Institute, Bozeman, MT, 2003).
32. M. R. Walter, D. J. Des Marais, *Icarus* **101**, 129 (1993).
33. W. N. Doemel, T. D. Brock, *Appl. Environ. Microbiol.* **34**, 433 (1977).
34. P. L. Siering *et al.*, *Geomicrobiol. J.* **23**, 129 (2006).
35. S. L. Cady, J. D. Farmer, in *Evolution of Hydrothermal Ecosystems on Earth (and Mars?)*, G. Bock, J. Goode, Eds. (J. Wiley and Sons, Chichester, UK, 1996), pp. 150–173.
36. S. Murchie *et al.*, *J. Geophys. Res.* **112**, E05S03 (2007).
37. R. E. Milliken *et al.*, Abstract P12A-02, presented at the American Geophysical Union Fall Meeting, San Francisco, CA, 10 to 14 December 2007.
38. This research was carried out for the Jet Propulsion Laboratory, California Institute of Technology, under a contract with NASA.

Supporting Online Material

www.sciencemag.org/cgi/content/full/320/5879/1063/DC1
Figs. S1 to S4
Table S1

18 January 2008; accepted 15 April 2008
10.1126/science.1155429

Formation of Box Canyon, Idaho, by Megaflood: Implications for Seepage Erosion on Earth and Mars

Michael P. Lamb,* William E. Dietrich, Sarah M. Aciego, Donald J. DePaolo, Michael Manga

Amphitheater-headed canyons have been used as diagnostic indicators of erosion by groundwater seepage, which has important implications for landscape evolution on Earth and astrobiology on Mars. Of perhaps any canyon studied, Box Canyon, Idaho, most strongly meets the proposed morphologic criteria for groundwater sapping because it is incised into a basaltic plain with no drainage network upstream, and approximately 10 cubic meters per second of seepage emanates from its vertical headwall. However, sediment transport constraints, ^4He and ^{14}C dates, plunge pools, and scoured rock indicate that a megaflood (greater than 220 cubic meters per second) carved the canyon about 45,000 years ago. These results add to a growing recognition of Quaternary catastrophic flooding in the American northwest, and may imply that similar features on Mars also formed by floods rather than seepage erosion.

A central thrust in geomorphology and planetary science is to link diagnostic landscape morphologies to formation processes. A prominent example is the formation of amphitheater-headed canyons, in which the stubby appearance of valley heads, steep headwalls, and little landscape dissection upstream have long been interpreted to result from seepage erosion or groundwater sapping on Earth (*1*–*4*), Mars (*5*, *6*), and now Titan (*7*). Theory (*8*), experiments (*9*), and field studies (*10*) have validated this hypothesis in unconsolidated sand, showing that valley heads are undermined and propagate upstream from seepage-induced erosion. This means that valleys can grow without precipitation-fed overland flow, which has profound implications for landscape evolution on Earth and the hydrologic cycle and habitability of Mars.

Despite widespread acceptance of the seepage-erosion hypothesis and its validation in sand, we lack an unambiguous example of an amphitheater-headed canyon formed by seepage erosion in bedrock because of overlapping features generated by rainfall runoff at most sites on Earth (*11*). Even the amphitheater-headed valleys of the Colorado Plateau and Hawaii, which are most often cited as classic examples of groundwater sapping in bedrock (*2*, *3*), have been in question because of evidence for flash floods and plunge-pool erosion (*11*–*13*). To better evaluate the seepage-erosion hypothesis, we set out to study the erosion and transport processes within a bedrock canyon, Box Canyon, Idaho, USA, which has a steep amphitheater-shaped headwall, contains the 11th-largest spring in the United States, and lacks the landscape dissection and rainfall runoff upstream of its headwall that has made other sites controversial (Fig. 1A). Moreover, Box Canyon exhibits remarkable similarity in morphology and possibly lithology (basalt) with many Martian canyons (Fig. 1B) that have been attributed to seepage erosion (*5*, *6*).

Box Canyon is located within the Snake River Plain, a broad and relatively flat basin in southern Idaho filled by sediments and volcanic flows that erupted over the course of ~15 million to 2 thousand years ago (ka) (*14*). Several tributaries of the Snake River Canyon appear as stubby valleys that end abruptly in amphitheater heads, including Malad Gorge, Blind Canyon, and Box Canyon (Fig. 2), all of which have been attributed to seepage erosion (*1*, *4*). Box Canyon is cut into the Sand Springs Basalt [also named the Basalt of Rocky Butte (*15*); see supporting online material (SOM) text] with an Ar-Ar eruption age of 95 ± 10 ka (*16*) and U-Th/He eruption ages that range from 86 +12 ka to 130 ± 12 ka (*17*), and this basalt filled an ancestral canyon of the Snake River (*18*).

Department of Earth and Planetary Science, University of California, Berkeley, CA 94720–4768, USA.

*To whom correspondence should be addressed. E-mail: mpl@berkeley.edu